MECHANICAL CHARACTERIZATION OF FLUORIDE OPTICAL FIBERS

R. El Abdi [a,*], A. Dumitrache Rujinski [b] and M. Poulain [c]

[a] Université de Rennes1, IPR, Département Mécanique &Verres–CS74205-35042 Rennes, France

[b] Universitatea Politehnica din Bucuresti, Splaiul Independentei, 313, IMST, 060042 Bucarest, Romania

[c] Université de Rennes1, Lab. Matériaux Photoniques – CS 74205 - 35042 Rennes, France

*Corresponding author; e-mail: relabdi@ univ-rennes1.fr; Tel & Fax: + 33 (0) 2 23 23 41 12

ABSTRACT

Mechanical dynamic tests were performed on fluoride glass fibers and silica optical fibers to examine the mechanical strength. These fibers were tested on ambient atmosphere and after aging in a vacuum desiccator with silica gel used as the desiccant.

A higher value of the ratio of Young's modulus to hardness indicates a greater tendency to plastic behavior in the case of fluoride fibers. For tensile tests, the strength of silica fiber is nine times greater than that of fluoride fiber and eight times greater in the case of bending tests. Aging in a desiccator decreases the residual water content and improves the fluoride fiber strength.

Keywords: Optical fibers, mechanical tests, fluoride glasses, failure strength.

1. INTRODUCTION

Fluoride glass fibers were first intensively developed for long distance telecommunication applications due to their ultra-low theoretical optical loss (0.001 dB/km). However these glasses are very susceptible to crystallization. Past researchers have shown that crystallization of these glasses is suppressed in microgravity and enhanced in hyper-gravity, showing a crystallization dependency on gravity. The specific material used for this research was a fluorozirconate glass, which is a subset of the Heavy Metal Fluoride Glasses family known as ZBLAN (ZrF_4, BaF_2, LaF_3, AlF_3, NaF). Such fibers can be doped with a number of rare earth ions for application in fiber lasers and amplifiers.

The main interest of fluoride glasses is associated with their potential in developing a new generation of optical waveguides which are superior to traditional SiO_2 optical fibers in their transparency range and their optical characteristics [1].

Comparing with silica fiber, the fluoride optical fiber has many unique characteristics, such as wide operating wavelength range (the wide range of infrared lights, visible lights and even ultraviolet lights) and high emission efficiency when rare-earth elements are doped into, especially excellent emission characteristic with Tm doped ZBLAN fiber [2- 5].

As a promising host material, ZBLAN glass used in fluoride fibers has been attracting great interest for up-conversion luminescence because it is relatively easy to prepare, and more importantly has a very low multiphonon relaxation rate [6- 9].

Because of the highly ionic bond character, fluorides tend to have low phonon energies (~500 cm^{-1}) compared to many oxides such as silica based glasses (~1200 cm^{-1}). This low phonon energy causes the infrared (IR) absorption edge of fluorides to have a higher wavelength than silica glasses and allows fluorides to function as effective windows beyond the 4 mm IR cut-off observed in fused silica.

Silica glass, the most common optical fiber material is certainly robust, having high tensile strength and resistance to thermal shock [10].

However, silica has a spectral window of only 0.3 to 2 μm and is virtually opaque to wavelengths longer than 2 μm. It also suffers from laser-induced damage at quite low power [11, 12].

Fluoride optical fiber have a large-band transmission from 0.3 μm to 4.3 μm [13- 15].

Fluoride glass fibers are less robust than silica but can nevertheless be made in multi-kilometer lengths, sufficiently strong to be spooled and handled. Some are attacked by water but the effect is minimized in suitable compositions. Fluoride glasses are generally resistant to radiation damage [16- 18], though rare earth doping may lower the damage threshold [19].

The main problem with the fiber is its poor mechanical strength. Degradation may be due to attack by atmospheric moisture or stresses and cracks introduced into the fiber during drawing and spooling or to damage which was not removed after drilling. The intrinsic strength of a glass, its real strength, depends on minor flaws. Considerable effort was made to remove scratches.

Even one remaining crack is sufficient to precipitate the eventual complete rupture of the fiber. Such cracks would probably be opened up and propagated by low level heating and applied stress [10].

Many studies were undertaken concerning optical and chemical properties of fluoride fibers, but very few studies have been carried out on their mechanical behavior when subjected to bending or tensile tests due to their poor mechanical strength.

Two-point bending is the simplest technique for the measurement of failure strains of glass fibers under a variety of experimental conditions.

Tang et *al* [20] use two point bending technique to evaluate the failure strains, under both inert and ambient conditions, for a number of conventional glasses (commercial silica, soda-lime

silicate, and E-glass). But no experimental mechanical study of very brittle fibers such as fluoride fibers was presented until then.

In this work, tensile and two point bending tests were performed on fluoride and silica fibers for different displacement velocities. A theoretical study is proposed to understand the mechanical behavior of each fiber. Some fibers were aged in a desiccator before undergoing mechanical tests.

2. OPTICAL FIBERS USED

2.1 Fluoride optical fiber

The multimode fluoride fiber has an operating wavelength between 0.3 and 4.3 µm. The combined coating diameter is 220 µm with a diameter clad of 150 µm and a core diameter of 100 µm (Fig.1). The operating temperature is from -180°C to 150°C. This fiber has a numerical aperture of 0.2 (NA value). Attenuation was ≤ 0.1 dB/m [3.4 - 3.6 µm]. Elastic properties of cladding and core for the studied optical fiber of compositions (mol%) $53ZrF_4$-$20BaF_2$-$4LaF_3$-$3AlF_3$-20NaF are given in Table 1.

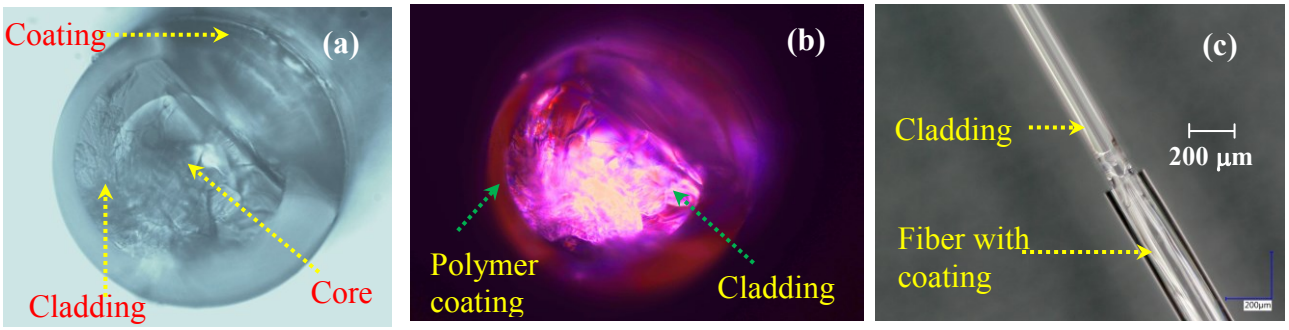

Fig. 1. Fluoride fiber: a): three components, b): Fiber crossed through light, c) fiber with removed coating

Table 1. Elastic constants of cladding and core of used fluoride fiber

Material	Density kg/cm^3	Young's modulus GPa	Shear modulus GPa	Poisson's ratio	Bulk modulus (GPa)
Cladding	4735	54.35 ± 6.10	20.56 ± 0.86	0.322 ± 0.039	50.8 ± 6.04
Core	4375	53.39 ± 6.36	20.37 ± 0.29	0.311 ± 0.037	46.9± 5.59

The elastic parameters of the glass below were obtained by measurement of sound velocities using the longitudinal and transverse velocities:

$$E = \rho.\ (V_T)^2 \quad \frac{3.(V_L)^2 - 4.(V_T)^2}{(V_L)^2 - (V_T)^2} \tag{1}$$

$$G = \rho.\ (V_T)^2 \tag{2}$$

$$\upsilon = \frac{(V_L)^2 - 2.(V_T)^2}{2.\left((V_L)^2 - (V_T)^2\right)} \tag{3}$$

$$K = \rho.\ \frac{3.(V_L)^2 - 4.(V_T)^2}{3} \tag{4}$$

where V_L and V_T are the longitudinal and transverse velocities respectively. ρ is the density obtained by electronic densimeter, E is the Young's modulus, G is the shear modulus, ν is the Poisson's ration and K is the bulk modulus.

2.2 Silica optical fiber

The used multimode silica optical fiber has two acrylate coatings (primary and outer coatings) (Fig. 2). This fiber has a numerical aperture of 0.2 (NA value) with an operating wavelength of 850/1300 nm. A soft, primary coating has a low module of elasticity, adheres closely to the glass fiber and forms a stable interface. It protects the fragile glass fiber against micro-bending and attenuation. The outer coating protects the primary coating against mechanical damage and acts as a barrier to lateral forces. It has a high glass transition temperature and Young modulus. It has good chemical resistance and serves as a barrier against moisture [21- 23]. The combined coating diameter is 245 μm, the silica core has a diameter of 50 μm and the clad diameter is 125 μm (Fig. 2).

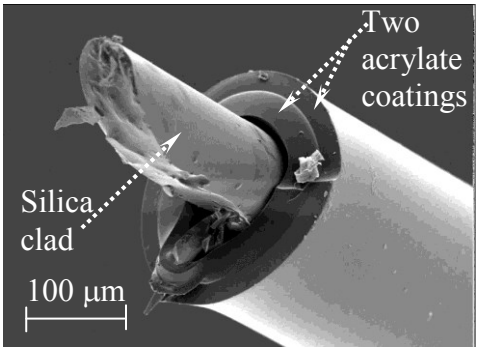

Fig. 2. Silica optical fiber used

3. TEST BENCHES USED

3.1 Bending test bench

While the bending method does not replace tensile testing as a fiber strength measurement technique, it presents attractive features and advantages, providing valuable information about flaw size distribution [24]. In our case, the ease and the duration of the testing and the small effective length of the fiber sample made the bending test one of the most appropriate choices for investigation.

The ‘‘as-received’’ fibers and those aged in a desiccator were subsequently put through dynamic tests using a two-point bending testing device (Fig. 3). The fiber package was cut into two 8 cm length parts.

Special care was required to prevent the fiber slipping during the faceplate displacement and to maintain the fiber ends in the same vertical plan.

The two points bending bench is made up of a displacement plate which is mounted on an aluminium plate (Fig. 3a). The first thrust block is movable and mounted on the displacement plate, while the second thrust block is fixed on a force sensor. The optical fiber is positioned between the two thrust blocks in such a way that it forms a "U". To avoid slipping, the fiber is positioned in the grooves of the thrust blocks (Figs. 3b, 3c).

During the test, load and displacement are recorded, allowing the load/displacement curve to be obtained. At breaking point, the stress applied to the fiber was deduced using the distance d between the two faceplates (Fig. 3c). A non-linear relation defined by Proctor and improved by Griffioen [25] can give the evolution of the stress σ (GPa) as a function of second polynomial order i.e.:

$$\sigma = E \ . \varepsilon \left(1 + \frac{\alpha'' . \varepsilon}{2} \right) \tag{5}$$

with

$$\alpha'' = \frac{3}{4}\alpha + \frac{1}{4} \tag{6}$$

where α is a non-linear elastic parameter (typical value of α is 6 for the most optical fibers [26, 27]). The strain ε was defined by:

$$\varepsilon = 1.198 \left[\frac{d_f}{d - d_c + 2d_g} \right] \tag{7}$$

where E is the Young modulus, d_c is the polymer coating diameter, d_f is the fiber diameter, $2d_g$ is the total depth of the 2 grooves and d is the distance between the two faceplates (Fig. 3c).

Initially, the distance between the two plates (fixed block and movable plate), between which the optical fiber is placed, is 10 mm. The movable plate moves to the left and thereby compresses the fiber which breaks in its middle. The load gradually increases when the movable plate moves closer to the fixed block and the load decreases drastically after the fiber breaks. The distance *d* between the two parts of the fiber at rupture is equal to: 10 mm minus the distance covered by the movable plate before fiber breaking.

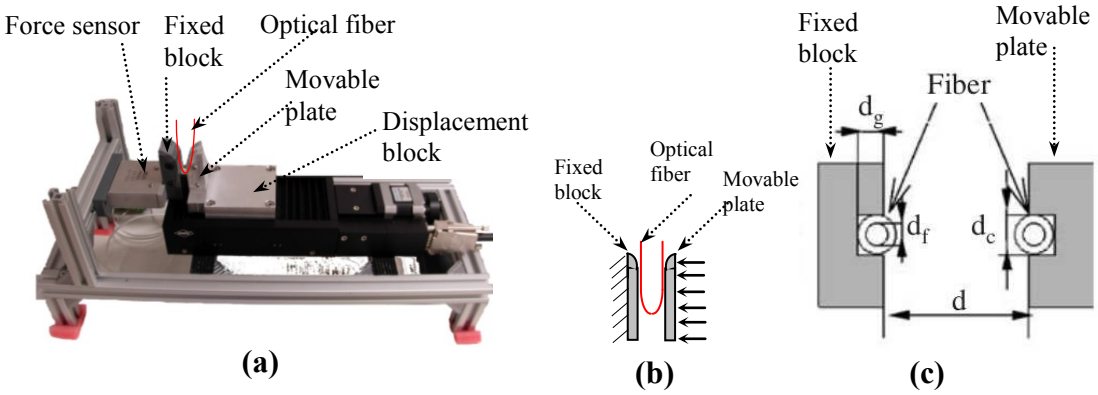

Fig. 3. (a) Bending bench used; (b) and (c) fiber between thrust blocks.

3.2 Tensile bench used

The dynamic tensile test consists of subjecting fibers to a deformation under a constant velocity until rupture. The fiber is rolled three times around two pulleys (Fig. 4); the lower pulley is fixed and the upper pulley is movable with different velocities (0.8, 2.6, 4.4, 6.2 and 8 mm/s). These strain rates, expressed as a percentage of the initial sample length (200 mm), correspond to 4 10^{-3} s^{-1}, 13 10^{-3} s^{-1}, 22 10^{-3} s^{-1}, 31 10^{-3} s^{-1} and 40 10^{-3} s^{-1}. This represents the minimum and maximum deformation velocity for optical fibers subjected to stretching in telecommunication networks.

Tensile testing was performed in a controlled environment with 46-52% relative humidity with a maximum of 5 % humidity variation for each series of the tensile tests.

During the test, the tensile load was measured using a dynamometric cell (load sensor) while the fiber deformation was deduced from the displacement between the fixed lower pulley and the mobile higher pulley (Fig. 4).

The testing procedure used 20 samples for each velocity.

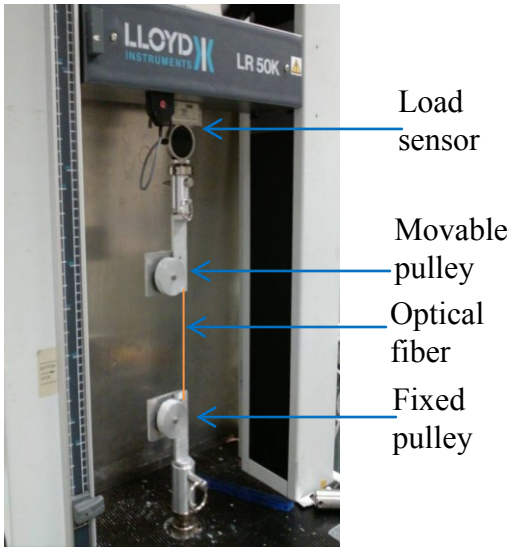

Fig. 4. Tensile test bench used

4. RESULTS and DISCUSSION

4.1 Bending tests

Figure 5 shows the change of the failure distance between the plates when the fluoride fiber was subjected to the two point bending test for different faceplate velocities.

It is noted that the failure distance between the two plates decreases according to their velocity. Indeed, the fluoride fiber is very brittle and breaks for large curvature radii when placed between the two plates.

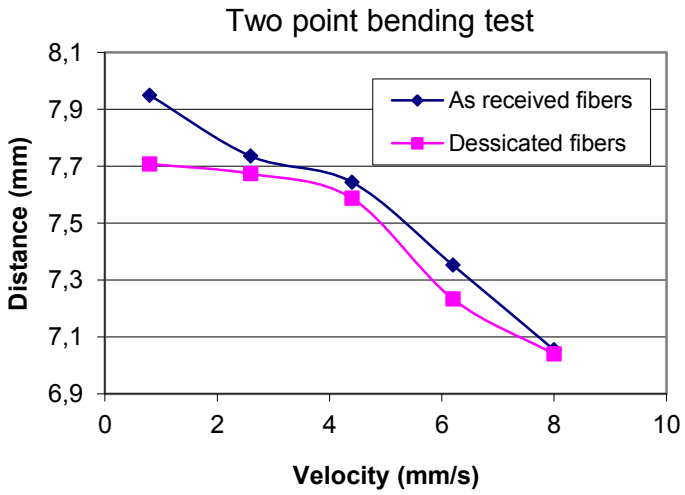

Fig. 5. Failure distance for fluoride fiber under two point bending test

The stiffness k of the fiber is given as following [25]:

$$k = \pi.r^4.E.\sqrt{1-\left[\alpha''.r/2.R\right]^2}\ /4 \qquad (8)$$

in which R is the fiber's bending radius and r is the radius of the fiber's cross-sectional area (Fig. 6).

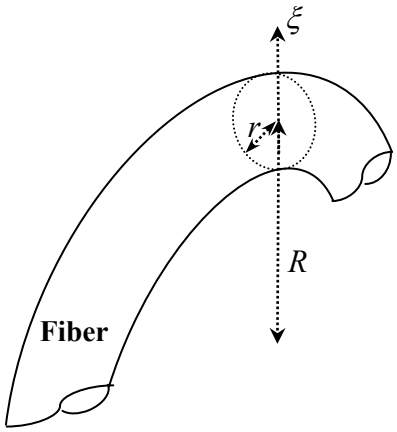

Fig. 6. Schematic view of a bent fiber

The fiber breaks for large curvature radii R, and Eq. (8) shows that the fiber stiffness k is initially high at the beginning of the displacement of the faceplates and thus the rupture occurs quickly. When placing the fluoride fibers in the desiccator for one week in order to maintain them in a dry atmosphere, some residual water was removed and this leads to partial micro-crack closures. This allows the fiber to bend more and a smaller failure distance between the plates was obtained (Fig. 5). Thus, the failure fiber force for the desiccated fiber was a little higher than that of an 'as received fiber' (Fig.7).

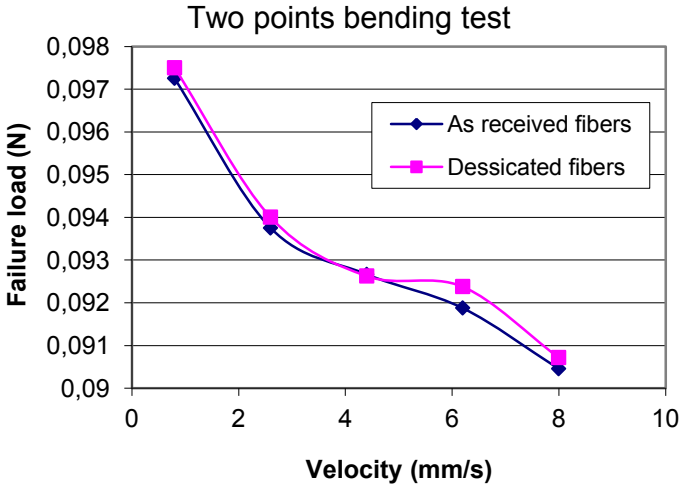

Fig. 7. Failure load for fluoride fiber under two point bending test

Silica fiber tolerates more bending than the fluoride fiber. The failure distance for the silica fiber is on average 5 times smaller than that of fluoride fiber (Fig. 8). Silica fiber can endure smaller curvature radii than the fluoride fiber and therefore will break for loads which are 8 times higher (Fig. 9).

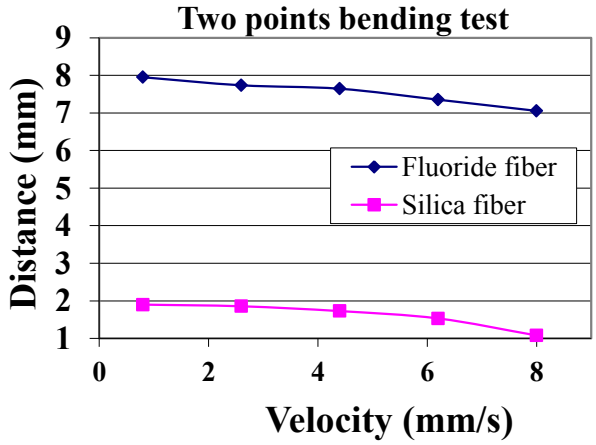

Fig. 8. Faceplates distance at failure for silica and fluoride fibers

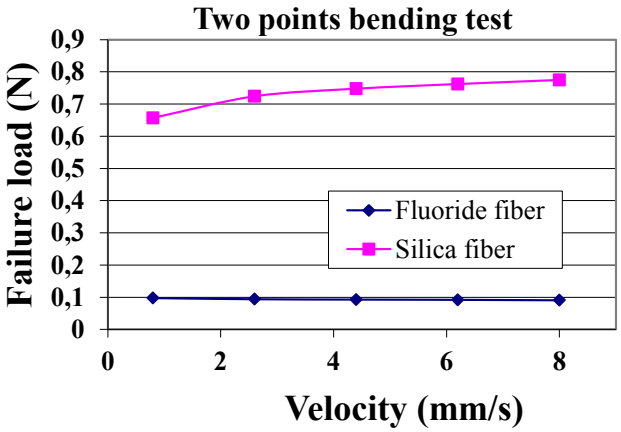

Fig. 9. Failure load for silica and fluoride fibers for different faceplate velocities

The stress of an optical fiber subjected to bending between two plates at each part of the bent fiber is equal to [25]:

$$\sigma(\xi) = E.\left[\frac{\xi}{R} + \frac{1}{2}.\alpha''\left(\frac{\xi}{R}\right)^2 - \frac{1}{8}.\alpha''\left(\frac{r}{R}\right)^2 - \frac{1}{8}.\left(\frac{r}{R}\right)^2\right] \qquad (9)$$

The maximum stress $\sigma(\xi)_{max}$ was obtained for $\xi = r$ (Fig. 6):

$$\sigma(\xi)_{max} = \sigma(r) = E.\left[\frac{r}{R} + \frac{1}{2}.\alpha''\left(\frac{r}{R}\right)^2 - \frac{1}{8}.\alpha''\left(\frac{r}{R}\right)^2 - \frac{1}{8}.\left(\frac{r}{R}\right)^2\right] \quad (10)$$

$$\sigma(r) = E.\left[\frac{r}{R} + \frac{3}{8}.\alpha''\left(\frac{r}{R}\right)^2 - \frac{1}{8}.\left(\frac{r}{R}\right)^2\right] \quad (11)$$

For α'' equal to 4.75 (using $\alpha = 6$ in Eq. 6), Eq. (11) leads to:

$$\sigma(r) = E.\left[\frac{r}{R} + \frac{53}{32}.\left(\frac{r}{R}\right)^2\right] \quad (12)$$

One can note that for silica optical fibers under bending tests, when the plate velocity was small, the failure distance was large (Fig. 8), thus the movable plate (Fig.3) had covered a small distance. That led to a large curvature radius R and then the maximum stress was small (Eq. 12). For that reason, an increase of the failure force according to plate velocity was obtained (Fig. 9). It was not the case for fluoride fibers where failure stresses decrease according to plate velocities (Fig. 7). As mentioned above, fluoride fibers contain many flaws, impurities and microcracks introduced during drawing and spooling [10] even if many efforts were made to remove these flaws. The fluoride fibers having defects with sizes a few nanometers cannot be represented by Eqs. 9-12. These equations are valid for a continuous medium without defects. The silica fibers have fewer intrinsic micro-defects than the fluoride fibers and the stresses inside silica fibers can be modeled by Eq. 11.

4.2 Tensile tests

Figure 10 shows the tensile failure strength for the fluoride fibers subjected to tensile tests at different faceplate velocities. The tensile bench determines the velocity to the upper pulley (movable pulley) (Fig. 4). It follows that the higher the velocity was, the higher the failure load. The experimental results can be smoothed by a quadratic polynomial form.

Figure 11 shows that the higher the velocity was, the greater the tensile force, and therefore the failure distance was small. The fiber elongation had a linear change according to the movable pulley velocity.

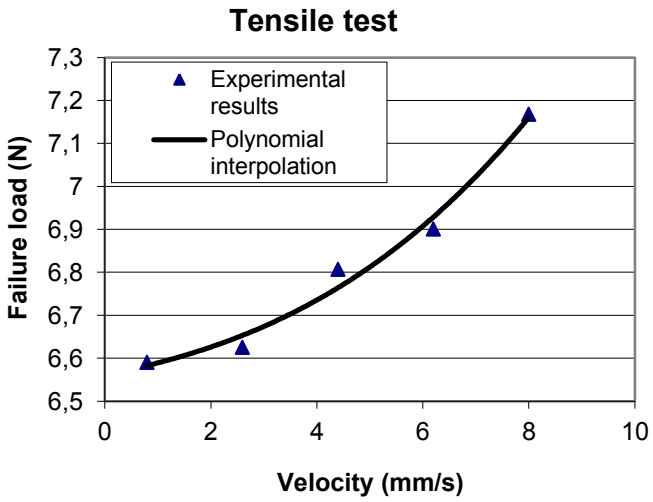

Fig. 10. Failure load for fluoride fiber under tensile test for different faceplate velocities

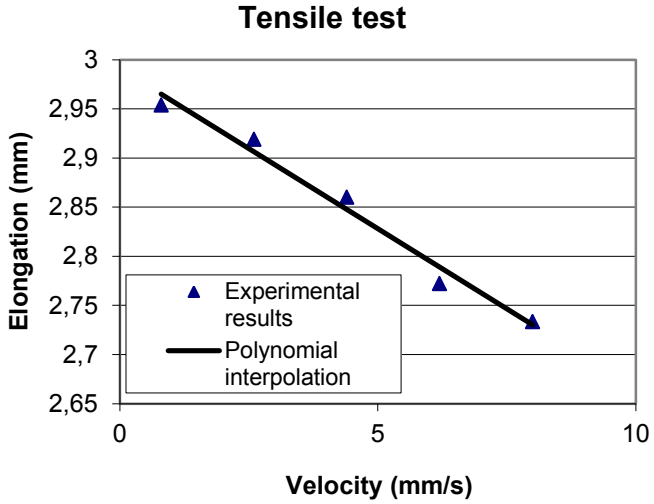

Fig. 11. Elongation for fluoride fiber under tensile test for different faceplate velocities

Figure 12 compares the failure forces for silica and fluoride fibers submitted to tensile tests. Table 2 gives some physical properties of fluoride and silica fibers. Young's modulus of silica fibers was higher than that of the fluoride fibers (Table 2). Therefore, failure strength of silica fibers was higher than that of fluoride fibers, even if the cladding diameter of fluoride fiber was greater than that of the silica fiber (Fig. 13). The failure load for the silica fiber was, on average, 9 times higher than that of the fluoride fiber (Fig. 12).

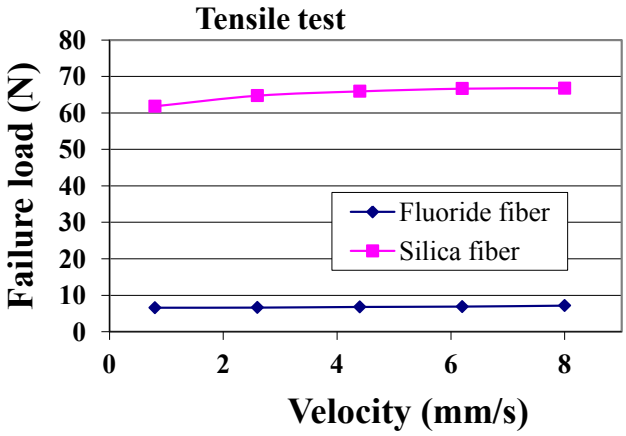

Fig. 12. Failure load for fluoride and silica fibers under tensile test for different faceplate velocities

Table 2. Physical properties of silica and fluoride glasses

Parameters	Silica	Fluoride
Young's Modulus E (GPa)	72	55
Knoop Hardness H (GPa)	7.7	2.2
Shear modulus (GPa)	29.5	20.5
E/H	9.4	24
Glass Transition Temperature (°C)	1100-1700	257
Melting Temperature (°C)	1721	450

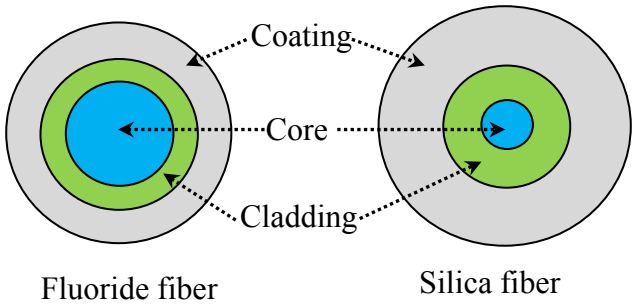

Fig. 13. Schematic sizes of fluoride and silica fibers

4.3 Mechanical strength of fluoride fiber

The main problem with the fluoride fiber is its poor mechanical strength. Degradation may be due to attack by atmospheric moisture or stresses and cracks introduced into the fiber during drawing and spooling [10]. Whatever the intrinsic strength of a glass, its actual strength depends on minor flaws. It operates on the ''weakest link'' principle.

The Hillig and Charles model [28] considers that crack blunting can occur due to plastic or viscous deformation as well as corrosion (Fig. 14). When under strain, if the stress at crack tip is not enough to cause plastic flow, it is possible for the crack to sharpen due to corrosion until the plastic yield stress is reached [29]. On the other hand, for the fluoride fiber, a higher value of the ratio of Young's modulus to hardness (E/H) was obtained (Table 2) and indicates greater tendency to plastic behavior. So, a crack blunting (Fig.14) can easily take place for fluoride fiber.

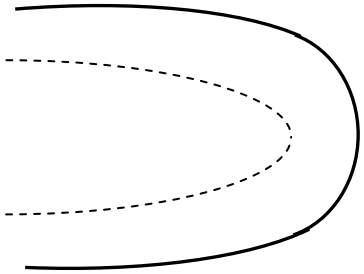

Fig. 14. Crack blunting for fluoride fiber

5. CONCLUSION

The difficulty for testing fluoride fibers was due to their fragility and their cost. Indeed, the fluoride fibers are more expensive than silica fibers and one must take a lot of care to minimize sample losses during testing. Furthermore, their fragility involves frequent breaking before the beginning of bending or tensile tests. Although the pulley diameters for the traction bench were quite large, the winding of fluoride fiber around the pulley must be done slowly to avoid handling or compression of another portion of the fiber already wound around the pulley.

In addition, fluoride fibers have many intrinsic defects that are not uniformly distributed. The number of testing experiments was quite high because many fiber failures occur around the pulley and not in the middle of the part of fiber between the two pulleys during the tensile test.

The bending test also required high accuracy. The setting of the fiber between two plates hed to be done slowly and a few seconds before the start of the dynamic test. A fiber which was left for a long time between the plates broke before the test starts.
The silica fiber, which is more flexible than the fluoride fiber, was easier to test.

Although the fluoride fiber has very interesting optical properties, it remains very sensitive to humidity. Even if the residual moisture was reduced, the fiber strength increased only very

moderately. In addition, tests should be performed within a few minutes of the fiber being removed from the desiccator.

The tensile tests showed that fluoride fiber elongation decreased with increasing velocity. On the other hand, the failure loads remained much lower than that of the silica fiber.
Finally, fluoride fibers had a higher value of the ratio of Young's modulus to hardness (E/H) which led to crack blunting.

REFERENCES

1. J. Lucas. Fluoride glasses for modern optics. J. of Fluorine Chemistry 1995; 72: 177-181.
2. V. Nazabal, M. Poulain, M. Olivier, P. Pirasteh, P. Carny, J.L. Doualan, S. Guy, T. Djouama, A. Boutarfaia, J. L. Adam. Fluoride and oxyfluoride glasses for optical applications. J. of Fluorine Chemistry 2010; 134: 18-23.
3. X. Zhu and N. Peyghambarian, High power ZABLAN glass fiber lasers: Review and prospect. Adv. Optoelectron. 2010; 2010: 1-2.
4. J. Méndez-Ramos, P. Acosta-Mora, J. C. Ruiz-Morales, M. Sierra, A. Redondas, E. Ruggiero, L. Salassa, M. E. Borges, P. Esparza, Rare-earth doped colour tuneable up-conversion ZBLAN phosphor for enhancing photocatalysis. Optical Materials 2015; 41: 98-103.
5. W. Su, S. Lou, H. Zou, B. Han, Highly birefringent ZBLAN photonic quasi-crystal fiber with four circular air holes in the core. Infrared Physics & Technology 2014; 66: 97-102.
6. H. Yang, J. Gao, Different dynamics of ultraviolet up-conversion in Tm^{3+}: ZBLAN glass under blue laser excitation. Physica B 2014; 426: 31-34.
7. F. Auzel, Y. H. Chen, Experimental determination of exponential parameters for multiphonon residual absorption in a ZBLAN: Er^{3+} fibre. Optical and Quantum Electronics 1994; 26: S559-S563.
8. J. Méndez-Ramos, P. Acosta-Mora, J. C. Ruiz-Morales, T. Hernandez, M. E. Borges, P. Esparza, Heavy rare-earth doped ZBLAN glasses for UV-blue up-conversion and white light generation. J. of Luminescence 2013; 143: 479-483.
9. C. He, D. Zhao, G. Qin, K. Zheng and W. Qin, Enhanced ultraviolet up-conversion luminescence of Tm and Yb codoped ZrF_4-BaF_2-LaF_3-AlF_3-NaF Glass, J. Nanosci. Nanotechnol. 2011; 11: 9494-9497.

10. P. McNamara, D. G. Lancaster, R. Bailey, A. Hemming, P. Henry, R. H. Mair. A large core microstructured fluoride glass optical fibre for mid-infrared single-mode transmission. J. of Non-Crystalline Solids 2009; 355: 1461–1467.
11. S.W. Allison, G.T. Gillies, D.W. Magnusson, T.S. Pagano. Pulsed laser damage to optical fibers. Appl. Opt. 1985; 24 (19): 3140.
12. L. Sudrie, M. Franco, B. Prade, A. Mysyrowicz. Study of damage in fused silica induced by ultra-short IR laser pulses. Opt. Commun. 2001; 191: 333.
13. V. Lambin-Iezzi, S. Loranger, M. Saad, R. Kashyap, Stimulated Brillouin scattering in SM ZBLAN fiber. J. of Non-Crystalline Solids, 2013; 359: 63-68.
14. M. Poulain, J. Lucas, Verres fluorés au tétrafluorure de zirconium. Propriétés optiques d'un verre dopé au Nd^{3+}. Mater. Res. Bull. 1975; 10: 243–246.
15. D. Hewak, R. Deol, J. Wang, G. Wylangowski, J. Mederios Neto, B. Samson, R. Laming, W. Brocklesby, D. Payne, A. Jha, Low phonon-energy glasses for efficient 1.3 μm optical fibre amplifiers, Electron. Lett. 1993; 29: 237–239.
16. T. Yamashita. Recent advances in IR-transmitting fibers for laser power delivery. Review of Laser Engineering 1999; 27 (3): 167-72.
17. M. Doshida, K. Teraguchi, M. Obara. Gain measurement and up-conversion analysis in Tm^{3+}, Ho^{3+} co-doped alumino-zirco-fluoride glass. IEEE Journal of Quantum Electronics 1995; 31 (5): 910-915.
18. Y. Feng, X. Chen, F. Song, K. Li, G. Zhang. Upconversion luminescence of ZBLAN: Tm^{3+}, Yb^{3+} glass pumped by a ~970 nm LD and its concentration effect. Proc. SPIE 1998; 3551: 116.
19. A. Chandonnet, P. Laperle, S. LaRochelle, R. Vallée. Photodegradation of fluoride glass blue fiber laser. Proc. SPIE 1997; 2998: 70-81.
20. Z. Tang, N. P. Lower, P. K. Gupta, C. R. Kurkjian, R. K. Brow, Using the two point bending technique to determine failure stress of pristine glass fibers. J. of Non Crystalline Solids 2015; 428: 98-104.
21. I. Severin, R. El Abdi, M. Poulain and M. Caramihal. Reliability evolution of optical fibre subjected to chemical environment. Applied Mechanics and Materials 2012; (152-154): 414-147.
22. V. Chean, R. El Abdi and J.C. Sangleboeuf. Water effect on interfacial adhesion of an optical fiber embedded in a composite material. J. of Composite Materials, 2014; 48 (18): 2273-2280.

23. R. El Abdi, A. Dumitrache Rujinski and M. Poulain. Effects of immersion duration and temperature on mechanical properties of optical fibers aged in CTAC aqueous solution. Engineering Science and Technology (An International Journal) 2015; 18: 52-58.
24. M. J. Mathewson, C. R. Kurkjian and S. T. Gulati. Strength measurement of optical fibres by bending. J. Am. Ceram. Soc. 1986; 69 (11): 815–821W.
25. W. Griffioen. Optical fiber reliability. Thesis edited by Royal PTT Netherlands NV, PTT Research, Leidschendam, 1994.
26. F.P. Mallinder and B.A. Proctor. Elastic constants of fused silica as a function of large tensile strain. Phys. Chem. Glasses 1964; 5 (4): 91.
27. G.S. Glaesemann, S.T. Gulati, J.D. Helfinstine. Effect of strain and surface composition on Young's modulus of optical fibers. Techn. Digest, 11th OFC, 1988; TUG5: 26.
28. W. B. Hilling and R. J. Charles. Surfaces, stress-dependent surface reactions and strength. High Strength materials, V. F. Zachey, ed. New-York: Wiley 1965; 682-701.
29. J. Colaizi, M. J. Matthewson. Mechanical durability of ZBLAN and aluminum fluoride based optical fiber. J. of Lightwave Techn. 1994; 12 (8): 1317-1324.